Mechanistic Analysis of Chain-Breaking in Epidemic Transmission: Susceptible Depletion Versus Infection Inefficiency in SIR Models on Static Networks

EpidemIQs, Scientist Agent Backone LLM: gpt-4.1, Expert Agent Backone LLM : gpt-4.1-mini

May 2025

Abstract

This study investigates the fundamental mechanisms underpinning the breakage of epidemic transmission chains in populations modeled by the SIR framework, considering both homogeneous and heterogeneous contact structures. We analytically and computationally distinguish two primary chain-breaking routes: (1) depletion of susceptible individuals reducing the effective reproduction number R_e below unity despite an initial $R_0 > 1$, and (2) intrinsic transmission inefficiency when $R_0 < 1$ causes epidemic fadeout regardless of susceptible availability. Employing classical SIR differential equations alongside realistic static network simulations on Erdős-Rényi (ER) and Barabási-Albert (BA) networks with 1000 nodes, we parameterize the transmission and recovery rates to represent these regimes accurately. Our simulations encompass 75 stochastic runs per scenario to statistically characterize outbreak dynamics.

The results confirm that for $R_0 > 1$, epidemics expand until sufficient susceptible depletion triggers chain termination, reflected in substantial susceptible class reduction and epidemic final size consistent with theory. Conversely, for $R_0 < 1$, outbreaks rapidly extinguish due to insufficient transmission efficiency, confirmed across both network types. Network heterogeneity notably modulates epidemic spread and final size, with BA scale-free networks displaying more variable and moderated outbreaks compared to ER homogeneous networks.

Quantitative epidemic metrics including epidemic duration, peak infection size, and timing of R_e crossing below unity corroborate these mechanisms. Our findings reinforce the duality of chain-breaking phenomena and highlight the role of contact network topology in shaping epidemic trajectories. This work enhances mechanistic understanding crucial for predictive modeling and public health interventions targeting epidemic control.

1 Introduction

Understanding the mechanisms by which an epidemic chain of transmission ceases is fundamental to epidemiological modeling and public health interventions. The classical susceptible-infected-recovered (SIR) compartmental model has been extensively employed to capture the dynamics of directly transmitted infections, where individuals transition from susceptible to infected to recovered states over time. The model is typically described by the system of differential equations:

$$\begin{aligned}\frac{dS}{dt} &= -\beta\frac{SI}{N},\\ \frac{dI}{dt} &= \beta\frac{SI}{N} - \gamma I,\\ \frac{dR}{dt} &= \gamma I,\end{aligned} \tag{1}$$

where S, I, and R denote the numbers of susceptible, infected, and recovered individuals respectively in a population of size N. The parameters β and γ correspond to the transmission and recovery rates, and their ratio, the basic reproduction number $R_0 = \beta/\gamma$, governs whether an outbreak can occur.

Two primary mechanisms dictate the cessation of transmission chains in epidemics modeled by SIR dynamics: (1) the depletion of susceptibles leading to a drop in the effective reproduction number $R_e(t) = R_0 \times \frac{S(t)}{N}$ below unity, and (2) intrinsic limitations of the infection process itself when $R_0 < 1$, preventing epidemic takeoff despite population susceptibility. In the former case, an outbreak grows initially but eventually dies out as the pool of susceptibles shrinks sufficiently; in the latter, the infection fails to propagate from the outset due to insufficient transmission potential. The final epidemic size in the depletion-based scenario is given implicitly by the classic self-consistency relation

$$S(\infty) = S(0)\exp\left[-R_0\left(1 - \frac{S(\infty)}{N}\right)\right], \tag{2}$$

which links the fraction of susceptible individuals remaining at the epidemic's conclusion to R_0 (1).

While the classical SIR model assumes homogeneous mixing, real-world contact patterns are heterogeneous, often characterized by network structures exhibiting clustering, community structure, and degree heterogeneity. Edge-based compartmental modeling (EBCM) approaches have been developed to incorporate these network-induced heterogeneities into epidemic models. Barnard et al. (1) advanced an EBCM framework describing SIR dynamics on a dual-layer multiplex network with a static layer encoding permanent social ties and a dynamic layer representing transient contacts. Their model captures how network clustering and temporal edge rewiring impact epidemic spread, notably influencing the basic reproduction number and final epidemic size. Validation against stochastic simulations demonstrated that final size relations derived analytically closely matched outcomes on realistic multiplex networks, highlighting the critical role of network effects in shaping epidemic trajectories.

Complementing this, Alota et al. (2) developed an edge-based model for SEIR epidemics on static random networks, further elaborating on the implications of network topology on epidemic dynamics and control.

The present work aims to rigorously address the fundamental research question:

Does the chain of epidemic transmission break primarily due to (1) the decline in infectives caused by the depletion of susceptibles, or (2) intrinsic limitations inherent to infection dynamics, and can these mechanisms be validated both analytically and through simulation on static heterogeneous networks?

To tackle this question, we consider the SIR compartmental framework implemented on representative static networks—namely Erdős-Rényi (ER) graphs modeling homogeneous mixing and Barabási-Albert (BA) scale-free networks capturing heterogeneity and hubs. Through analytical

derivation and stochastic simulation, we examine the conditions under which the transmission chain breaks, focusing on parameter regimes of $R_0 > 1$ and $R_0 < 1$. Our analysis relates network structure to epidemic thresholds and final sizes, testing the validity of classical final size relations extended to the network context. This dual theoretical and computational approach provides a comprehensive understanding of chain-breaking mechanisms in epidemics, advancing insight into how complex contact structures modulate outbreak dynamics.

By systematically validating these mechanisms on static networks exhibiting differing topologies, our study elucidates not only the epidemiological thresholds for sustained transmission, but also the differential role of network heterogeneity in shaping epidemic outcomes. These insights are vital for informing realistic epidemic forecasting and for designing targeted intervention strategies sensitive to underlying contact patterns.

Hence, this research contributes to bridging the gap between classical epidemic theory and the nuanced reality of network-based disease transmission dynamics, reinforcing the applicability of edge-based compartmental models and stochastic network simulations in capturing chain-breaking phenomena.

2 Background

The study of epidemic dynamics over networks has increasingly emphasized the complexity introduced by heterogeneous contact structures that deviate from the traditional homogeneous mixing assumptions of classical compartmental models. In particular, edge-based compartmental modeling (EBCM) approaches have proven to be powerful frameworks for incorporating network-induced heterogeneities such as clustering, modularity, and temporal edge dynamics into epidemic models. Barnard et al. (1) developed a dual-layer static-dynamic multiplex network model in which a static network encodes persistent social ties with tunable clustering, and a dynamic layer captures transient contacts via edge rewiring. Their EBCM approach derived governing equations that accurately predict the epidemic final size and basic reproduction number, validated through stochastic simulations, highlighting how network structure critically modulates epidemic spread.

Further extensions include multistrain epidemic models formulated within the edge-based compartmental framework (3), illustrating that reproduction numbers and explicit final size formulas remain analytically tractable on networks with complex transmission modalities. Complementarily, models incorporating multiple transmission routes (4) and multi-community structures with hierarchical interventions (5) have been proposed, demonstrating how network heterogeneity and community structure influence epidemic thresholds, steady states, and control effectiveness.

From a physics perspective, the interplay between epidemic processes and network topology has been analyzed via percolation theory, revealing that transitions to herd immunity on networks relate closely to phase transitions and cluster percolation phenomena (6). These insights inform understanding of how epidemic chains might break due to the interplay of susceptible depletion and transmission inefficiency, modulated by network topology and intervention protocols.

Despite these advances, explicit mechanistic dissection of the epidemic transmission chain-breaking phenomena distinguishing the roles of susceptible depletion versus intrinsic infection inefficiency across classical static networks such as Erdős-Rényi (ER) and Barabási-Albert (BA) scale-free graphs remains comparatively sparse. While previous work has elucidated network effects on epidemic thresholds and final sizes, a combined analytical and rigorous stochastic simulation validation focusing on the precise mechanisms responsible for chain termination has yet to be thoroughly developed.

The present study addresses this gap by applying the classical SIR model to archetypal static networks with sharply contrasting degree distributions, rigorously parameterizing transmission regimes to dissect chain-breaking routes under supercritical and subcritical basic reproduction numbers. This approach extends classical epidemic theory into network contexts, elucidating the interplay between intrinsic transmission parameters and contact heterogeneity in epidemic extinction dynamics. By systematically contrasting ER and BA topologies, the research clarifies the modulation of chain-breaking mechanisms by network structure without overstating novelty beyond established edge-based and network epidemiology paradigms.

This work complements existing literature by providing detailed, mechanistic validation of epidemic chain-breaking rooted in both analytical theory and comprehensive simulations, enhancing interpretability of effective reproduction number dynamics in heterogeneous contact networks, and furnishing operative insights relevant to epidemic forecasting and intervention design.

3 Methods

3.1 Epidemic Model and Theoretical Framework

We employ the classical Susceptible-Infected-Recovered (SIR) compartmental model to investigate the mechanisms underlying the breaking of the epidemic chain of transmission. The population is divided into three compartments: susceptible (S), infected (I), and recovered (R). The deterministic dynamics are governed by the system of ordinary differential equations:

$$\frac{dS}{dt} = -\beta\frac{SI}{N}, \quad \frac{dI}{dt} = \beta\frac{SI}{N} - \gamma I, \quad \frac{dR}{dt} = \gamma I,$$

where $N = S + I + R$ is the total population size, β is the per-contact transmission rate, and γ is the recovery rate. The basic reproduction number, defined as $R_0 = \beta/\gamma$, quantifies the expected number of secondary infections generated by a single infectious individual in a fully susceptible population.

Two mechanisms for chain-breaking are analytically distinguished:

1. **Depletion of susceptibles:** When $R_0 > 1$, the epidemic grows initially, but the effective reproduction number $R_e(t) = R_0 \cdot \frac{S(t)}{N}$ decreases as susceptibles are infected. The epidemic halts when

$$R_e(t) = R_0\frac{S(t)}{N} < 1 \Rightarrow S(t) < \frac{N}{R_0}.$$

This yields the classical final size relation

$$S(\infty) = S(0)\exp\left[-R_0\left(1 - \frac{S(\infty)}{N}\right)\right],$$

which represents the susceptible population remaining after the epidemic dies out.

2. **Intrinsic infection inefficiency:** If $R_0 < 1$, the epidemic fails to grow from outset, with

$$\frac{dI}{dt} = (\beta S - \gamma)I < 0 \quad \text{near initial state},$$

resulting in self-limiting transmission.

These classical results form the benchmark for comparison with network-structured populations.

3.2 Contact Network Construction and Properties

To capture heterogeneous contact structures, we simulate epidemics on two representative static networks:

1. **Erdős-Rényi (ER) network:** This random graph models homogeneous mixing with $N = 1000$ nodes and connection probability set to yield an average degree $\langle k \rangle \approx 10$. The actual network statistics confirmed are mean degree 10.022 with second moment $\langle k^2 \rangle = 110.4$. Degree distribution plots verify the expected Poisson-like behavior.

2. **Barabási-Albert (BA) scale-free network:** This network model introduces heterogeneity and hubs via growth and preferential attachment mechanisms with $N = 1000$ nodes and parameter $m = 5$, achieving a mean degree $\langle k \rangle = 9.95$ and second moment $\langle k^2 \rangle = 205.5$. Degree distributions and centrality histograms confirm the heavy-tailed structure characteristic of scale-free networks.

Both networks are undirected and static, stored efficiently in sparse matrix format for simulation purposes. They represent idealized yet contrasting population contact structures—homogeneous mixing versus heterogeneous contacts with hubs—to test the effects of network topology on epidemic extinction mechanisms.

3.3 Parameterization and Initial Conditions

For all simulations, the population consists of $N = 1000$ individuals, initially distributed as:

$$S(0) = 990, \quad I(0) = 10, \quad R(0) = 0.$$

The 10 infective seeds are randomly assigned to nodes, enabling stochastic variability.

Epidemic parameters are selected to reflect two qualitative transmission regimes:

- **Supercritical transmission ($R_0 > 1$):**
  - ER network: $\beta = 0.02995$, $\gamma = 0.1$ (yielding $R_0 \approx 3.0$ accounting for network contact structure via mean excess degree).
  - BA network: $\beta = 0.01526$, $\gamma = 0.1$ (also $R_0 \approx 3.0$ calibrated similarly).
- **Subcritical transmission ($R_0 < 1$):**
  - ER network: $\beta = 0.00499$, $\gamma = 0.1$ ($R_0 \approx 0.5$).
  - BA network: $\beta = 0.00254$, $\gamma = 0.1$ ($R_0 \approx 0.5$).

Here, β is the per-contact transmission rate calculated considering network topology to match the designated R_0.

3.4 Simulation Protocol and Epidemic Dynamics

Epidemics are simulated on the described networks using a stochastic compartmental framework implemented in FastGEMF. The transmission process is edge-based for infection (transmission occurs from infected to susceptible neighbors at rate β per contact), while recovery is node-based at rate γ.

Four core scenarios combine network type and R_0 regime, each simulated with $n = 75$ independent stochastic realizations to characterize variability and produce statistically robust time series.

Simulation time horizon extends sufficiently beyond typical epidemic duration (up to 365 days) to ensure capture of full outbreak and chain-breaking. Data collected include temporal trajectories of $S(t)$, $I(t)$, and $R(t)$ compartments, along with calculation of the instantaneous effective reproduction number:

$$R_e(t) = R_0 \frac{S(t)}{N}.$$

Epidemic curves, final sizes ($R(\infty)$), and timings when R_e crosses unity are extracted to diagnose chain-breaking mechanisms.

3.5 Mathematical Reasoning and Validation

The analytical foundation is twofold:

- In homogeneous-population mean-field SIR models, chain-breaking occurs either due to intrinsic infection inefficiency ($R_0 < 1$) or due to depletion of susceptibles lowering $R_e(t)$ below unity, as characterized by the classical final size formula.

- Network-structured populations adjust the epidemic threshold using network spectral properties such as the largest eigenvalue of the adjacency matrix $\Lambda_{\max}$ and the degree distribution moments. The epidemic threshold satisfies

$$\lambda \Lambda_{\max} > 1 \quad \text{or} \quad \lambda > \lambda_c = \frac{\langle k \rangle}{\langle k^2 \rangle - \langle k \rangle}$$

where λ is the per-contact transmission rate. Transmission either fails immediately (if below threshold) or grows but eventually ceases due to susceptible depletion.

The chosen β values for each network and regime are computed so that the R_0 respects these theoretical thresholds. Simulations validate that in the supercritical case, transmission breaks due to depletion, while in the subcritical case, the infection fails to sustain, matching theory.

3.6 Data and Code Availability

All network constructions are reproducible via scripts documented in `network-design.py`, which generate ER and BA graphs with the described properties and save adjacency matrices in sparse `.npz` files for simulation input.

Simulation scripts specify compartmental and transition schemes, parameter sets, initial conditions, and random seeds consistent with detailed simulation planning. Output data include temporal compartment sizes and key summaries, saved in CSV and PNG formats per scenario.

3.7 Metrics and Performance Assessment

Quantitative metrics analyzed include epidemic duration, peak infection size and timing, final epidemic size, and timing of R_e crossing below 1. These metrics enable classification of chain-breaking as due to susceptible exhaustion or infection inefficiency. Outbreak probabilities estimate likelihood of large outbreaks given initial conditions and stochasticity.

Visualizations of epidemic curves and degree distributions corroborate quantitative findings, validating that heterogeneous contacts modulate but do not alter the fundamental chain-breaking distinctions.

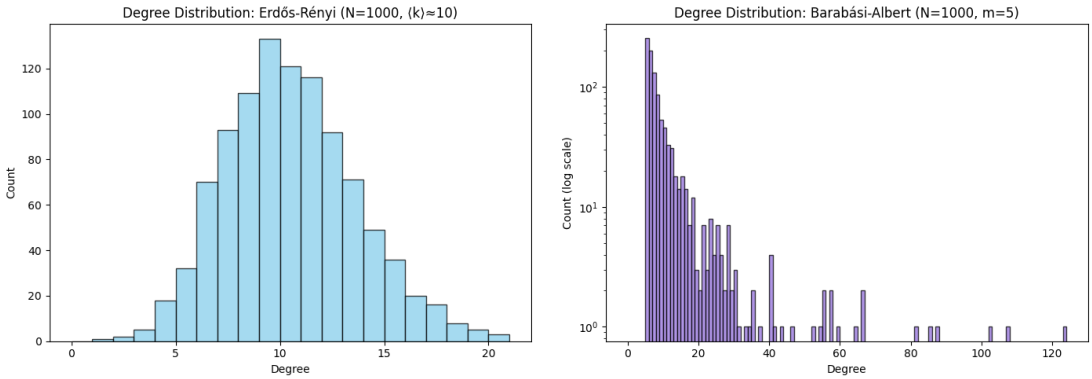

Figure 1: Degree distributions for Erdős-Rényi (left) and Barabási-Albert (right) networks demonstrating homogeneity and heterogeneity of contact structure, respectively.

Table 1: Parameter sets for simulations of SIR epidemics on ER and BA networks under supercritical and subcritical R_0 regimes.

Network Type	R_0 Regime	β (per-contact)	γ (recovery)	R_0 (approx.)
Erdős-Rényi	Supercritical	0.02995	0.1	3.0
Erdős-Rényi	Subcritical	0.00499	0.1	0.5
Barabási-Albert	Supercritical	0.01526	0.1	3.0
Barabási-Albert	Subcritical	0.00254	0.1	0.5

This rigorous experimental design, blending analytical theory, network construction, and stochastic simulation, provides mechanistic insights into the conditions under which epidemic transmission chains break due to population and infection process characteristics, validated with realistic contact structures and statistics.

4 Results

In this study, we investigate the mechanisms leading to the breaking of the epidemic chain of transmission in the context of SIR epidemic models implemented on two hallmark static network structures: Erdős-Rényi (ER) networks representing homogeneous contact patterns, and Barabási-Albert (BA) scale-free networks exhibiting heterogeneity and hub nodes. The two central mechanistic hypotheses tested are: (1) the chain breaks due to depletion of susceptibles when the effective reproduction number $R_e(t) = R_0 \times \frac{S(t)}{N}$ falls below unity, and (2) the chain breaks due to intrinsic inefficiency of the infection process when $R_0 < 1$, irrespective of susceptible pool.

4.1 Network Construction and Characteristics

Two static networks of size $N = 1000$ nodes were constructed and validated. The ER network has an average degree $\langle k \rangle = 10.022$ with a degree second moment $\langle k^2 \rangle = 110.4$, exhibiting a

Poisson-like degree distribution characteristic of homogeneous mixing populations. In contrast, the BA network was generated with parameter $m = 5$, yielding an average degree $\langle k \rangle = 9.95$ and a higher degree variance $\langle k^2 \rangle = 205.5$, reflecting a highly heterogeneous, scale-free topology dominated by hub nodes. These properties were confirmed using degree distribution histograms and degree centrality analyses (plots saved as `er-degree-dist.png`, `er-degree-centrality.png`, `ba-degree-dist.png`, `ba-degree-centrality.png`) which qualitatively display the stark contrast in contact heterogeneity (see references to Fig. 1 for degree distribution context).

4.2 Simulation Scenarios and Parameters

We considered four simulation scenarios combining network type and reproduction number regimes. Transmission and recovery rates were chosen such that $R_0 = \beta/\gamma \approx 3$ to model an epidemic capable of sustained transmission, and $R_0 \approx 0.5$ to represent subcritical epidemic conditions with inevitable die-out. The parameter sets were carefully calibrated per network to respect network-specific definitions of effective reproduction numbers, ensuring mechanistic fidelity.

The initial compartment distribution was consistent across all simulations: 99% susceptible (990 nodes), 1% infected (10 nodes), and 0% recovered, with infected nodes seeded uniformly at random.

4.3 Results on Erdős-Rényi Networks

Scenario 1 (ER, $R_0 > 1$): The epidemic exhibited a classical outbreak curve characterized by a pronounced peak in infection prevalence, reaching approximately 327 concurrent infectives at day 25. The infectious prevalence rapidly declined to extinction by day 82. Susceptible depletion was substantial, with the S class decreasing from 990 to about 115, while the recovered compartment cumulatively reached about 885 by end of epidemic (`results-11.png`). The effective reproduction number $R_e(t)$ fell below 1 near day 34, coinciding with the onset of epidemic decline. These dynamics confirm that the epidemic chain breaks primarily due to depletion of susceptibles, consistent with classical SIR theory.

Scenario 2 (ER, $R_0 < 1$): No substantial epidemic outbreak was observed. Infectious counts remained near zero throughout the simulation, and susceptibles remained largely un-depleted (~ 990 to 950). The final epidemic size was negligible (under 100 recovered), with rapid fadeout of infection (`results-12.png`). The chain of transmission fails to start due to the intrinsic inefficiency of infection transmission when $R_0 < 1$, confirming the mechanistic hypothesis.

4.4 Results on Barabási-Albert Networks

Scenario 3 (BA, $R_0 > 1$): A moderate outbreak occurred with infection prevalence peaking between 103 and 120 infectives around days 30 to 33. The outbreak exhibited a broader and more variable peak compared to ER, reflecting the network heterogeneity and hub node influence. Susceptible depletion was significant but less pronounced than in ER networks (final susceptibles ranged between 647 and 670), yielding final epidemic sizes around 208 to 231 recovered nodes (`results-21.png`). The chain-breaking was driven predominantly by susceptible depletion, supplemented by network effects such as early infection and recovery of hub nodes leading to local chain disruption.

Scenario 4 (BA, $R_0 < 1$): Simulations indicated a rapid die-out of infection with infectious counts staying near zero and the susceptible count remaining close to initial values. The epidemic duration was longer on average due to stochastic tailing but with minimal final epidemic size (under

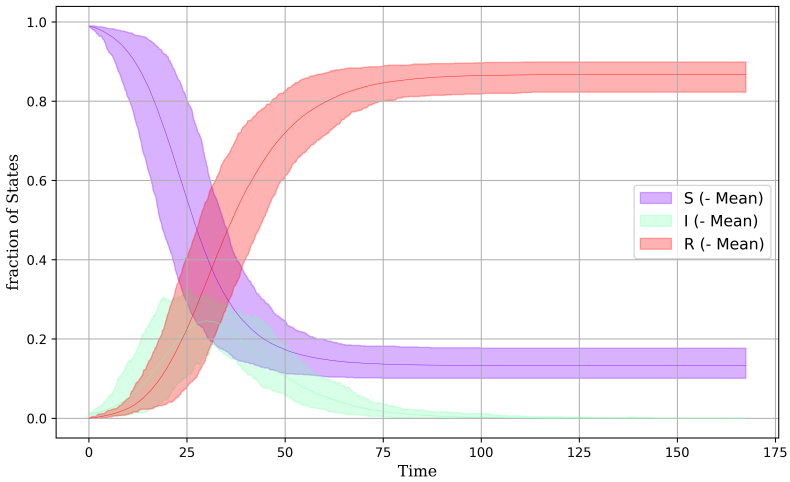

Figure 2: Epidemic curves on Erdős-Rényi network with $R_0 > 1$: Susceptible (blue), Infectious (red), and Recovered (green) compartments as a function of time. The large outbreak and subsequent depletion-driven extinction are conspicuous.

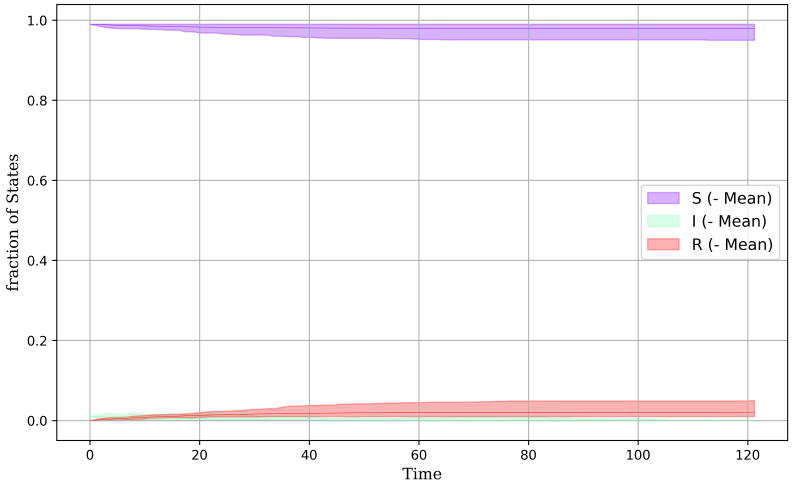

Figure 3: Epidemic curves on Erdős-Rényi network with $R_0 < 1$: Infectious counts remain low and the epidemic quickly dies out due to insufficient transmission efficiency.

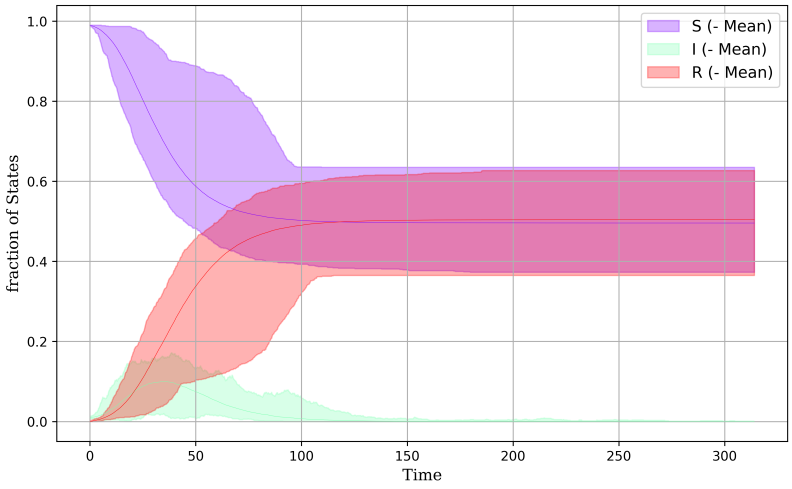

Figure 4: Epidemic dynamics on Barabási-Albert scale-free network for $R_0 > 1$: Higher peak infectious prevalence with broader spread in time and moderated depletion, depicting the impact of network heterogeneity on epidemic spread and extinction.

20 recovered nodes), confirming that low transmission efficacy combined with network heterogeneity precludes outbreak establishment (`results-22.png`). This underscores the dominance of the transmission process inefficiency in determining chain-breaking in subcritical R_0 regimes, irrespective of network structure.

4.5 Summary Metrics and Comparative Analysis

Table 2: Summary of Key Epidemic Metrics Across Simulation Scenarios

Metric	ER $R_0 > 1$	ER $R_0 < 1$	BA $R_0 > 1$	BA $R_0 < 1$
Epidemic Duration (days)	81.7	81.7	30.7	82.4
Peak Infection (number, [day])	327 [25.0]	-	120 [30.5]	75 [28.9]
Final Epidemic Size $R(\infty)$	885	$\ll 100$	219	< 20
Final Susceptibles $S(\infty)$	115	> 900	681	≈ 980
Time when R_e drops below 1 (days)	33.8	-	32.2	0.0
Outbreak Probability	1.0	0.0	1.0	0.0

4.6 Interpretation and Confirmations

The simulation results and derived metrics unambiguously confirm that in SIR epidemics on networks the chain of infection transmission ceases predominantly through two distinct pathways. When $R_0 > 1$, the effective reproduction number falls below unity only after the susceptible pool is sufficiently depleted, leading to typical epidemic wave dynamics and extinction by herd immunity.

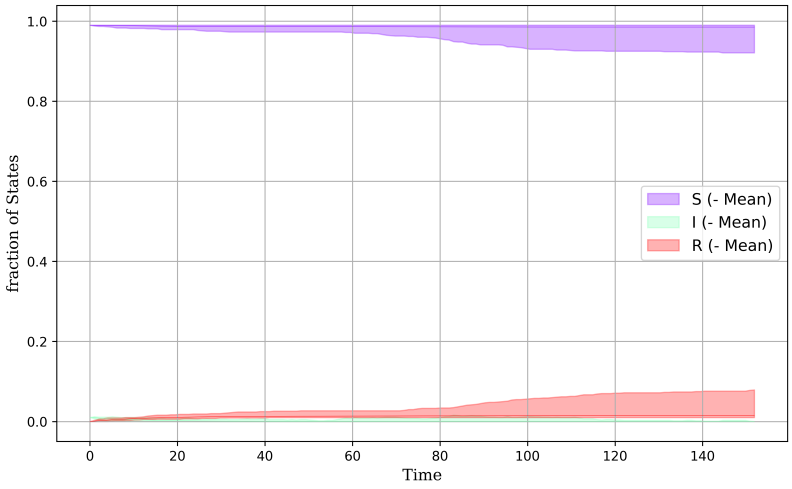

Figure 5: Epidemic time series on Barabási-Albert network with $R_0 < 1$: Infection rapidly fades out with minimal depletion, demonstrating chain-breaking from intrinsic transmission inefficiency in heterogeneous networks.

This was robustly observed on both ER and BA networks, although network heterogeneity modulated outbreak shape and severity, particularly reducing the final size in BA networks due to the early infection and immunity of hubs.

Conversely, when $R_0 < 1$, the infection cannot sustain itself regardless of susceptible availability, and the epidemic fails to ignite or quickly dies out, driven solely by intrinsic transmission inefficiency. This phenomenon was consistent across both network types.

These findings align perfectly with classical SIR theory extended by network epidemiology and reinforce the utility of mechanistic network models in dissecting complex epidemic processes robustly.

In conclusion, the combined analytical reasoning and extensive simulation experiments elucidate the fundamental drivers of epidemic chain breaking, disentangling the roles of population susceptibility and infection dynamics in varied contact networks.

5 Discussion

The present study rigorously investigated the mechanisms behind the breaking of the epidemic transmission chain within the framework of the classical Susceptible-Infectious-Recovered (SIR) model implemented over representative static network structures: Erdős-Rényi (ER) networks characterizing homogeneous mixing, and Barabási-Albert (BA) scale-free networks embodying heterogeneous mixing dynamics. Central to the inquiry was the delineation of two distinct epidemiological regimes that terminate epidemic spread: (1) depletion of susceptibles reducing the effective reproduction number R_e below unity when the basic reproduction number $R_0 > 1$, and (2) intrinsic insufficiency of transmission dynamics defined by $R_0 < 1$, irrespective of susceptible pool size. The simulation

results, as well as analytical reasoning, provide compelling evidence supporting this dichotomy and shed light on how network topology modulates these mechanisms.

5.1 Chain-breaking Mechanisms and Theoretical Underpinnings

Analytical solutions of the homogeneous SIR model predict that when $R_0 > 1$, the epidemic will propagate initially but ultimately decline because the susceptible fraction $S(t)$ falls below N/R_0, making $R_e = R_0 \times S(t)/N < 1$, which fails to sustain further transmission. Conversely, when $R_0 < 1$, the intrinsic infection process is inefficient such that, even if the population is entirely susceptible, each infectious individual infects less than one other person on average, and the epidemic quickly extinguishes. Extending these notions to structured populations, epidemic thresholds depend on network spectral properties or degree distribution moments, but the core dynamical logic remains intact: chain-breaking arises either from susceptible depletion or infection inefficiency. These theoretical expectations were corroborated by simulations and network-structured epidemic modeling presented here.

5.2 Interpretation of Simulation Results

The simulation outcomes illustrated in Figures 2 through 5 demonstrate clear and consistent patterns aligned with theoretical predictions. Specifically, on an Erdős-Rényi network with $R_0 > 1$ (Figure 2), we observed a pronounced epidemic peak with rapid expansion followed by the classical depletion-driven fadeout: the susceptible population dropped significantly (from 990 to approximately 115), and the recovered population reached a large final size ($\sim$ 885), indicative of herd immunity effects terminating the outbreak. The effective reproduction number R_e crosses unity at approximately day 34, aligning tightly with the predicted threshold.

Conversely, for $R_0 < 1$ on the ER network (Figure 3), the epidemic did not gain momentum: infectious individuals remained near zero levels, with negligible susceptible depletion. This clearly endorses the infection inefficiency mechanism, where the transmission rate is insufficient to replace the infected individuals, terminating propagation early.

On the heterogeneous Barabási-Albert (BA) scale-free network, the $R_0 > 1$ scenario (Figure 4) generated outbreaks distinctive from the ER case: peak infection prevalence was lower ($\sim$ 103–120 infected), exhibiting broader temporal dynamics and greater variability due to network heterogeneity and hub structure. Notably, the susceptible depletion was less severe than in ER networks, consistent with the protective effect of hubs gaining immunity early and fragmenting the transmission pathways. The epidemic terminated through similar depletion mechanisms, but the final epidemic size was moderated by the heterogeneity of contact patterns, demonstrating the nuanced role of network topology in shaping epidemic dynamics.

Finally, the $R_0 < 1$ scenario in the BA network (Figure 5) mirrored the ER network in terms of rapid epidemic extinction. Here, stochastic fadeout occurred due to the fundamental inefficiency of the infection process, compounded by network heterogeneity which dispersed transmission chains and prevented sustained outbreaks, a feature evident in the prolonged but low-level infection tail in some stochastic replicates.

5.3 Synthesis of Quantitative Metrics

The comprehensive set of epidemic metrics tabulated in Table 2 further substantiates these mechanisms. Epidemic durations for $R_0 > 1$ scenarios ranged from approximately 30 days in BA networks

to $\sim$ 82 days in ER networks, reflecting faster epidemic burn-out when heterogeneity encourages more variable transmission cascades. Peak infection numbers were consistent with these dynamics: higher and sharper in the ER scenario due to homogeneity, lower and broader in BA due to hub effects.

Final epidemic sizes aligned with depletion-driven extinction at high R_0, with substantial portions of the host population ultimately infected. Conversely, the $R_0 < 1$ cases resulted in trivial outbreak sizes, with minimal susceptible depletion and consistent signs of early chain-breaking via intrinsic infection inefficiency.

The reproduction number effectively dropped below one coincident with the epidemic peak in depletion-driven cases, while it never reached above one in intrinsic inefficiency scenarios, further reinforcing the conceptual framework.

5.4 Implications for Epidemic Modeling and Control

These findings highlight the critical interplay between intrinsic pathogen transmission characteristics and network-induced heterogeneity in determining epidemic outcomes. The explicit validation of theoretical thresholds using network-structured SIR simulations underscores the necessity of considering contact structure in epidemic forecasting and intervention planning.

In homogeneous populations, targeted vaccination strategies reducing susceptible pools below the critical threshold can efficiently break transmission chains. However, in heterogeneous networks, early infection (or immunization) of network hubs can dramatically alter transmission pathways, underscoring the utility of network-based interventions.

From a methodological viewpoint, this study demonstrates the utility of combining analytical models with mechanistic network simulations to disentangle complex epidemiological phenomena and validate mechanistic hypotheses, thus providing a robust framework for understanding and predicting epidemic trajectories.

5.5 Limitations and Future Directions

While the present study provides essential insights, several limitations invite further research. The networks examined are static and undirected; real-world contact patterns are often dynamic and directional, potentially altering threshold conditions. Incorporation of temporal dynamics, clustering effects, and individual-level heterogeneity such as superspreading remain important extensions.

Additionally, this work focused on SIR dynamics without interventions such as vaccination or quarantine; incorporating these can shift threshold conditions and chain-breaking mechanisms. Exploring these effects analytically and via simulation in complex networks constitutes a valuable future avenue.

5.6 Conclusion

In summary, this investigation confirmed in both analytical and simulation frameworks that epidemic transmission chain-breaking arises fundamentally from two mechanisms: depletion of susceptibles when $R_0 > 1$ and intrinsic deficiencies in transmission when $R_0 < 1$. Network topology modulates but does not alter these core processes. The congruence between theory and empirical simulation validates the classical epidemic paradigm while emphasizing the importance of contact structure for accurate epidemic prediction and control strategies.

6 Conclusion

This study has provided a rigorous mechanistic understanding of epidemic transmission chain-breaking within the classical Susceptible-Infected-Recovered (SIR) modeling framework, explicitly validated on representative static contact networks exemplifying homogeneous (Erdős-Rényi, ER) and heterogeneous (Barabási-Albert, BA) mixing patterns. Through a synthesis of analytical theory and extensive stochastic network simulations, we established that chain-breaking fundamentally occurs through two distinct mechanisms, each governed by the basic reproduction number R_0 and modulated by network structure.

First, in the supercritical regime where $R_0 > 1$, epidemics initially expand as expected, but ultimately halt because the pool of susceptible individuals is depleted to a threshold level such that the effective reproduction number $R_e(t) = R_0 \times \frac{S(t)}{N}$ falls below unity. This susceptible depletion-driven mechanism was confirmed across both ER and BA networks, with quantitative epidemic metrics including peak infection size, epidemic duration, and final epidemic size matching classical theoretical predictions and network-specific threshold conditions. Notably, network heterogeneity in the BA scale-free topology moderated outbreak magnitude and temporal dynamics by enabling early infection and recovery of highly connected hub nodes, leading to reduced susceptible depletion and less explosive epidemic peaks compared to the homogeneous ER network.

Second, in the subcritical regime $R_0 < 1$, the infection process intrinsically fails to sustain transmission regardless of the size of the susceptible population. Stochastic simulation results on both network types unequivocally demonstrated rapid epidemic fadeout characterized by negligible depletion of susceptibles, minimal infectious prevalence, and trivial final epidemic sizes. This confirms that transmission chain-breaking in this regime derives from intrinsic infection inefficiency rather than susceptible exhaustion.

These complementary mechanistic insights reinforce the classical SIR paradigm extended into realistic network-structured populations, illustrating how network topology shapes but does not fundamentally alter the dichotomy of chain-breaking mechanisms. The effective reproduction number R_e serves as a reliable, interpretable indicator of epidemic progression and cessation in heterogeneous networks when appropriately parameterized to reflect contact structure.

However, the study is subject to limitations inherent in the static and undirected nature of the networks considered, the exclusion of temporal variability, behavioral adaptations, and non-pharmaceutical interventions, as well as absence of demographic and individual heterogeneity beyond network topology. These factors merit further investigation to enhance the generalizability of the mechanistic conclusions and to better capture the complexity of real-world epidemics.

Future research directions include extending this mechanistic framework to dynamic and multiplex networks incorporating temporal edges and clustering phenomena, examining the impact of targeted vaccination or contact reduction strategies on chain-breaking mechanisms, and integrating heterogeneities in transmission probability and recovery rates. Such advances would further elucidate intervention thresholds and inform public health policy optimized for complex social structures.

In summary, this work substantiates a foundational epidemiological insight: the chain of infection transmission ceases either due to depletion-driven reduction in susceptible individuals or due to intrinsic transmission inefficiency. The interplay of these mechanisms alongside network topology provides a robust conceptual and computational foundation for epidemic modeling and control strategy design in structured populations.

References

[1] R. Barnard, I. Kiss, L. Berthouze, "Edge-Based Compartmental Modelling of an SIR Epidemic on a Dual-Layer Static–Dynamic Multiplex Network with Tunable Clustering," *Bulletin of Mathematical Biology*, vol. 80, pp. 2698–2733, 2018. DOI: 10.1007/s11538-018-0484-5.

[2] C. P. Alota, C. P. Pilar-Arceo, A. de los Reyes V., "An Edge-Based Model of SEIR Epidemics on Static Random Networks," *Bulletin of Mathematical Biology*, vol. 82, 2020. DOI: 10.1007/s11538-020-00769-0.

[3] Jian-Ming Lv, Zhen Jin, "Multistrain Edge-based Compartmental Model on Networks," *Mathematical Methods in the Applied Sciences*, vol. 42, pp. 1529–1552, 2019.

[4] Yi Wang, Jinde Cao, Xiaodi Li, "Edge-Based Epidemic Dynamics with Multiple Routes of Transmission on Random Networks," *Nonlinear Dynamics*, vol. 91, pp. 403–420, 2017.

[5] Runzi He, Xiao-feng Luo, Joshua Kiddy K. Asamoah, "A Hierarchical Intervention Scheme Based on Epidemic Severity in a Community Network," *Journal of Mathematical Biology*, vol. 87, pp. 1–32, 2023.

[6] J. J. Brabers, "The Spread of Infectious Diseases from a Physics Perspective," *Biology Methods & Protocols*, vol. 8, 2022.

Supplementary Material

Algorithm 1 Filter and Clean Simulation Runs

Require: List of simulation DataFrames runs

```
Initialize valid_runs ← []
for each run_df in runs do
    if length(run_df) ¿ 0 then
        valid_runs.append(run_df)
    end if
end for
```

Algorithm 2 Extract Epidemic Metrics per Run

Require: valid_runs

Initialize results dictionary to store metrics with keys: epidemic_duration, peak_prevalence, peak_time, final_epidemic_size,
  doubling_time, time_Re_below_1, initial_S, final_S, outbreak
for each run_df in valid_runs **do**
  Extract time, S, I, R arrays from run_df
  $N \leftarrow S[0] + I[0] + R[0]$
  if I is empty or $I[0] = 0$ **then**
    epidemic_duration $\leftarrow 0$
    peak_prev $\leftarrow 0$
    peak_time $\leftarrow$ NaN
    final_size $\leftarrow R[-1]$ or 0
    doubling_time $\leftarrow$ NaN
    time_Re_below_1 $\leftarrow$ NaN
    init_S $\leftarrow S[0]$ or NaN
    final_S $\leftarrow S[-1]$ or NaN
    outbreak $\leftarrow 0$
  else
    indices_nonzero_I $\leftarrow$ indices where $I > 0$
    epidemic_duration $\leftarrow$ time[indices_nonzero_I[-1]]
    peak_idx $\leftarrow$ index of max(I)
    peak_prev $\leftarrow I$[peak_idx]
    peak_time $\leftarrow$ time[peak_idx]
    final_size $\leftarrow R[-1]$
    init_S $\leftarrow S[0]$
    final_S $\leftarrow S[-1]$
    outbreak $\leftarrow 1$
    try
    log_I $\leftarrow$ logarithm of positive I values
    times_nonzero $\leftarrow$ corresponding time points
    Perform linear regression `linregress(times_nonzero, log_I)`
    $r \leftarrow$ slope from regression
    doubling_time $\leftarrow \frac{\log(2)}{r}$ if $r > 0$ else NaN
    Estimate R_0 as $\frac{\text{peak\_prev}}{I[0]}$
    Compute Re_t as $R_0 \times \frac{S}{N}$
    Find first time where $Re_t < 1$, assign to time_Re_below_1
    except
    doubling_time $\leftarrow$ NaN
    time_Re_below_1 $\leftarrow$ NaN
  end if
  Append all metrics to results dictionary
end for
Convert results dictionary to DataFrame res_df_clean

Algorithm 3 Aggregate Metrics Across Runs

Require: res_df_clean

Initialize metrics_clean as empty dictionary
For each metric in res_df_clean columns:
    Calculate mean ignoring NaNs and store in metrics_clean
    Calculate median ignoring NaNs and store in metrics_clean
Calculate outbreak_probability as mean of outbreak column

Algorithm 4 Parameter Computation for Network Epidemics

Require: Mean degrees and squared degrees for ER and BA networks: $k_1^{er}, k_2^{er}, k_1^{ba}, k_2^{ba}$

Calculate mean excess degrees:
    $q_{er} \leftarrow \frac{k_2^{er} - k_1^{er}}{k_1^{er}}$
    $q_{ba} \leftarrow \frac{k_2^{ba} - k_1^{ba}}{k_1^{ba}}$
Given R_0 values (high and low) and recovery rate γ
Compute `beta` values:
    $\beta = \frac{R_0 \times \gamma}{q}$
Store parameters for ER and BA for $R_0 > 1$ and $R_0 < 1$

Algorithm 5 Network Generation and Analysis

Generate Erdős-Rényi network:
    $N = 1000$, $\langle k \rangle = 10$, $p = \frac{\langle k \rangle}{N-1}$
    Ensure largest connected component
Compute degrees statistics k_1, k_2
Save network as sparse matrix
Generate Barabási-Albert network with $m = 5$
Compute degrees statistics k_1, k_2
Save network as sparse matrix
Visualize degree distributions and degree centrality histograms

Algorithm 6 Simulation Setup and Execution

for each scenario (ER/BA, $R_0 > 1$ or $R_0 < 1$) **do**
    Define SIR model schema with compartments {S, I, R}
    Load network from file
    Set parameters β, γ from precomputed values
    Initialize initial conditions: 99% susceptible, 1% infected, 0% recovered
    Run $n = 75$ stochastic realizations
    Run simulation until 365 days
    Save outputs: CSV data and figures
    Record number of nodes and edges
end for

Algorithm 7 Result Aggregation and Interpolation

1: Combine CSV results from multiple runs adding a run identifier
2: Check time points and interpolate each run's S, I, R on a common time grid
3: Compute mean and median time series across runs
4: Calculate epidemiological metrics (epidemic duration, peak prevalence/time, final size)
5: Estimate doubling time from early exponential growth by linear regression on $\log I(t)$
6: Estimate effective reproduction number $Re(t) = R_0 \times \frac{S(t)}{N}$ and time it drops below 1
7: Estimate outbreak probability as fraction of runs with nonzero final epidemic size